Electrochemical Cycling of Redox-Active Boron Cluster-Based Materials in the Solid State

Austin D. Ready,[a†] Ahamed Irshad,[b†] Anna Kallistova,[c] Moises Carrillo,[a] Milan Gembicky,[e] Ram Seshadri,[c,d] Sri Narayan,[b] Alexander M. Spokoyny*[a,f]*

[a]Department of Chemistry and Biochemistry, University of California, Los Angeles, Los Angeles, CA 90095, USA

[b]Department of Chemistry and Loker Hydrocarbon Research Institute, University of Southern California, Los Angeles, CA 90089, USA

[c]Materials Department and Materials Research Laboratory, University of California, Santa Barbara, Santa Barbara, CA 93106, USA

[d]Department of Chemistry and Biochemistry, University of California, Santa Barbara, Santa Barbara, CA 93106, USA

[e]Department of Chemistry and Biochemistry, University of California, San Diego, La Jolla, CA 92521, USA

[f]California NanoSystems Institute (CNSI), University of California, Los Angeles, CA 90095, USA

[†]These authors contributed equally

ABSTRACT: This work demonstrates the first successful electrochemical cycling of a redox-active boron cluster-based material in the solid state. Specifically, we designed and synthesized an ether-functionalized dodecaborate cluster, $B_{12}(OCH_3)_{12}$, which is the smallest redox-active building block in the $B_{12}(OR)_{12}$ family. This species can reversibly access four oxidation states in solution, ranging from a dianion to a radical cation. We show that a chemically isolated and characterized neutral $[B_{12}(OCH_3)_{12}]^0$ cluster can be utilized as a cathode active material in a PEO-based rechargeable all-solid-state cell with a lithium metal anode. The cell exhibits an impressive active material utilization close to 95% at C/20 rate, a high Coulombic efficiency of 96%, and reversibility, with only 4% capacity fade after 16 days of cycling. This work represents a conceptual departure in the development of redox-active components for electrochemical storage and serves as an entry point to a broader class of borane-based materials.

INTRODUCTION: In the past several decades, many researchers have advanced our knowledge of how carbon-based organic redox-active molecules can be incorporated into solid state battery materials.[1-8] Through solubility modifications via molecular weight, the addition of hydrophobic/hydrophilic groups, or impregnation in porous/polymeric materials, a number of redox-active small molecules (e.g., carbonyls, nitroxides, imides, disulfides, etc.) have been observed to retain their solution-phase redox activity in the solid state. Despite these advances, the incorporation of other well-defined covalent-based systems into electrochemically active materials in the solid state has been fundamentally underexplored. For example, polyhedral boron clusters, which are often described as three-dimensional aromatic analogues of benzene, can exhibit well-defined redox properties in solution, as seen for boranes ($[B_nH_n]^{2-}$; $n \leq 12$), carboranes, and their numerous functionalized derivatives.[9-45] Historically, a number of boron-based clusters have been deemed redox-inert species with wide electrochemical stability windows, prompting early studies

of $Li_2B_{12}Cl_{12}$ and $Li_2B_{10}Cl_{10}$ as novel electrolytes, first in $SOCl_2$[23, 46] and later in ethereal solvents.[47-49] More recently, there have been extensive efforts in developing some of these clusters for solid state electrolyte applications.[50-87]

Recent advances in boron cluster chemistry[44-45, 88-98] show that judicious exopolyhedral modifications of these species can result in the emergence of boron-centered redox events in solution, which in many cases can be tunable. In particular, ether-functionalized dodecaborate clusters [$B_{12}(OR)_{12}$; R = alkyl, aryl] demonstrate the richest solution-based redox behavior exhibited by boron clusters studied to date.[14, 95-97, 99-112] Due to the enhanced electronic stabilization provided by the ether groups, the majority of these boron clusters have access to four stable oxidation states in solution (Figure 1A). Their redox potentials can be tuned over a wide voltage range through simple modification of the electron-donating or withdrawing nature of the carbon-based substituent (Figure 1B). Specifically, our research group has studied these clusters as redox-active polymer dopants,[113-114] photooxidants,[103, 111] and electroactive species for redox-flow batteries.[108] Surprisingly, however, there have been no reports so far demonstrating that boron clusters in general have the ability to undergo redox processes in the solid state.

Due to their robustness[59-60, 115] and chemical tunability, polyhedral boron clusters present a potentially appealing platform for translating solution-phase redox behavior into solids. In this work, we describe for the first time the development of a model boron cluster-based system that can undergo reversible redox in the solid state. As a result, we show the successful incorporation of redox-active $B_{12}(OCH_3)_{12}$ into an electrochemical cell to demonstrate the feasibility of boron clusters for energy storage applications (Figure 1C).

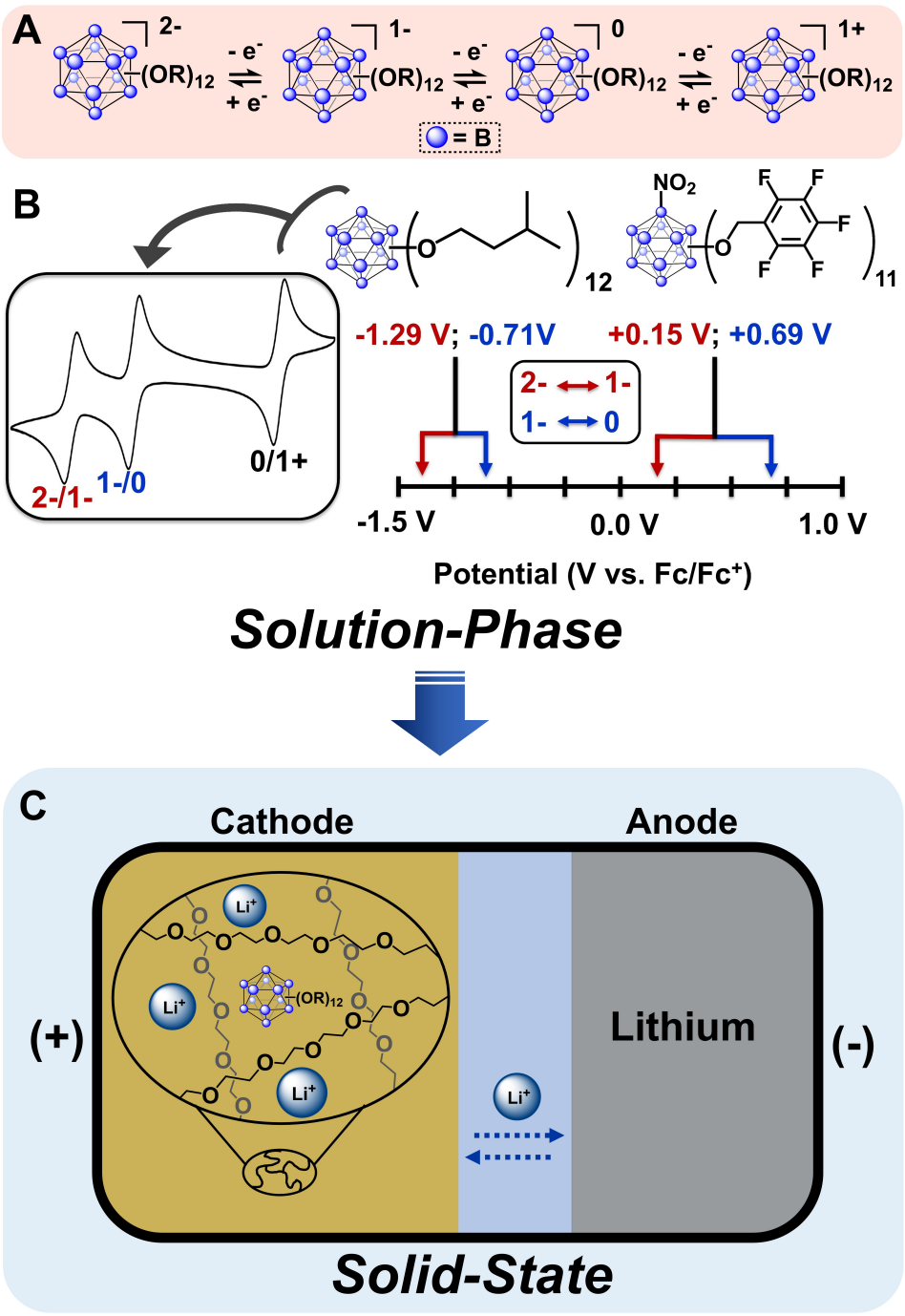

61

62 **Figure 1.** (A) Known reversible electronic transitions of $B_{12}(OR)_{12}$ clusters (B) Redox potentials

63 of two representative $B_{12}(OR)_{12}$ clusters; cyclic voltammogram of B_{12}(O-3-methylbutyl)$_{12}$ (inset)

64 (C) Depiction of a solid state electrochemical cell containing $B_{12}(OR)_{12}$ in a PEO matrix.

RESULTS & DISCUSSION: From a chemical design perspective, the ideal redox-active $B_{12}(OR)_{12}$ building block for electrochemical storage requires access to reversible, multi-electron redox, as well as a low molecular weight to ensure sufficient specific capacity. Furthermore, we hypothesize that in order to facilitate lithiation/delithiation, the oxygen atoms on the OR groups of the $B_{12}(OR)_{12}$ species should be sterically accessible to allow reversible metal ion coordination. All of these criteria exclude the previously developed alkylated and benzylated $B_{12}(OR)_{12}$ clusters studied thus far.

We hypothesized that the $B_{12}(OCH_3)_{12}$ cluster would serve as an ideal synthetic target for potential incorporation into a redox-active solid state material. Hawthorne and coworkers have previously reported the synthesis of this cluster[99] using a high-pressure reactor, starting from the tetrabutylammonium (TBA) salt of $[B_{12}(OH)_{12}]^{2-}$ and a large excess of methyl tosylate as a methylating agent. Importantly, the use of super stoichiometric amounts of methyl tosylate renders the purification of the final product cumbersome and reduces its overall purity. As such, we established a new facile microwave-assisted method to synthesize $B_{12}(OCH_3)_{12}$ (Figure 2A) using trimethylsulfoxonium bromide (TMSO-Br), which does not produce difficult to remove byproducts, allowing the cluster to be easily isolated. In a typical reaction, 60 mg of $TBA_2B_{12}(OH)_{12}$ is stirred with Hünig's base and 100 equivalents of TMSO-Br in air for 1 hour at 120°C in a microwave reactor, producing perfunctionalized $[B_{12}(OCH_3)_{12}]^{2-/1-}$, as judged by in situ ^{11}B NMR spectroscopy and mass spectrometry (SI, Figure S1-S4). Full methoxylation of all twelve boron vertices is confirmed when numerous peaks in the ^{11}B NMR spectrum (indicating partial substitution/desymmetrization of the cluster) coalesce to a broad singlet at -17 ppm.

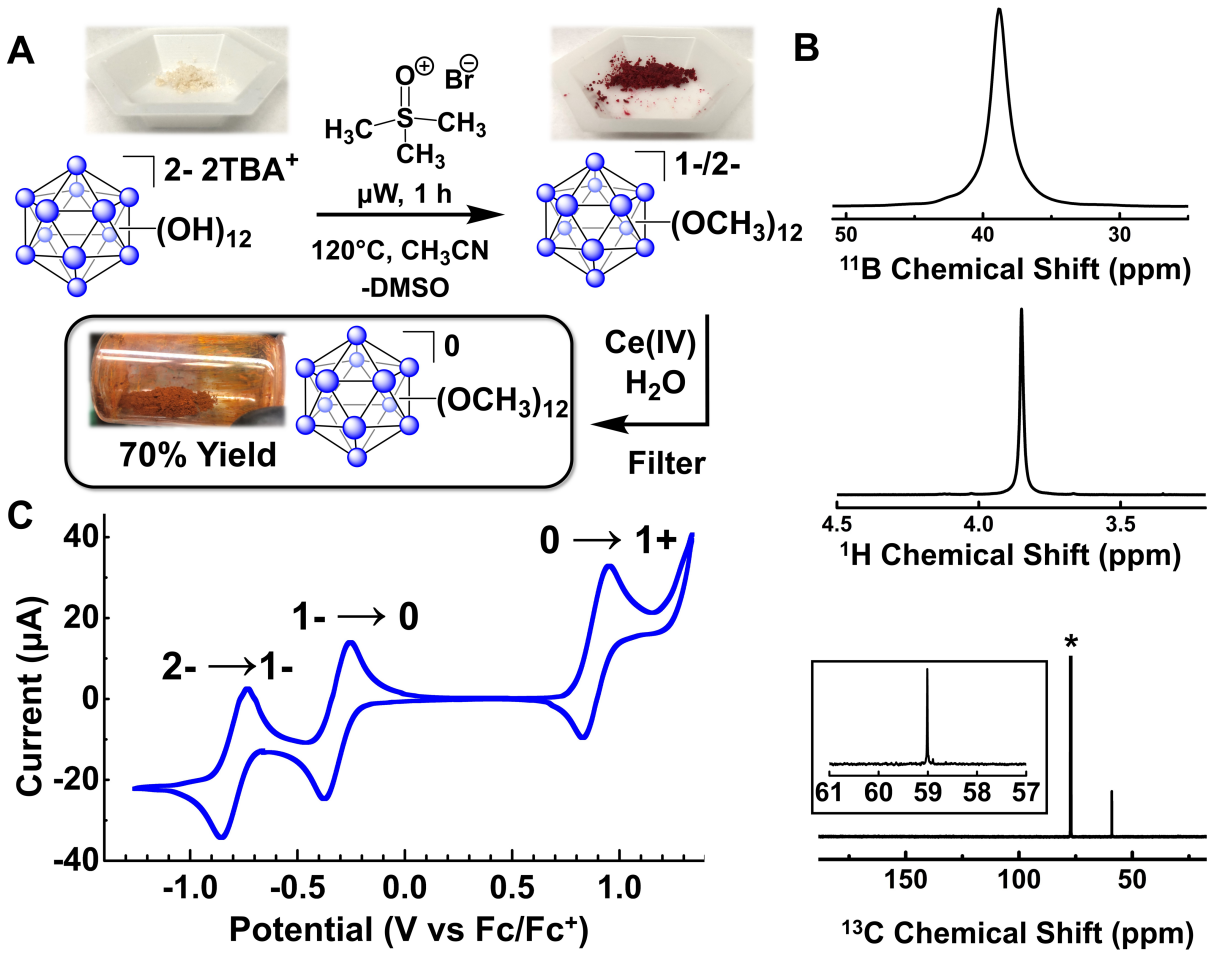

86

87

88 **Figure 2.** (A) Microwave-assisted synthesis of $[B_{12}(OCH_3)_{12}]^{1-/2-}$, followed by chemical oxidation.
89 (B) ^{11}B, ^{1}H, and ^{13}C NMR spectra, respectively, of $[B_{12}(OCH_3)_{12}]^{0}$ in $CDCl_3$ (asterisk represents
90 solvent) (C) Cyclic voltammogram of $B_{12}(OCH_3)_{12}$ in DCM.

91 Upon mixing $[B_{12}(OCH_3)_{12}]^{2-/1-}$ with an aqueous solution of Ce(IV), the original ^{11}B NMR
92 signal at -17 ppm disappears, with a concomitant emergence of a new signal at 38 ppm (Figure
93 2B), consistent with the formation of a neutral $B_{12}(OCH_3)_{12}$ species, which immediately
94 precipitates as an orange solid. This material is then subjected to a simple purification via filtration
95 and solvent washes. The complete removal of cerium salts is confirmed by XPS (SI, Figure S18)

and electrochemical characterization of the resulting product (Figure 2C). The chemical structure and oxidation state assignment of $B_{12}(OCH_3)_{12}$ were confirmed through multiple characterization methods, including solution-phase NMR spectroscopy (^{11}B, ^{13}C, ^{1}H) (Figure 2B), mass spectrometry (SI, Figure S1 and S2), and single crystal and powder X-ray crystallography (Figure 3). The high symmetry of the dodecaborate cluster is exemplified by the single resonance observed via ^{11}B, ^{13}C, and ^{1}H NMR spectroscopy (Figure 2B; SI, Figure S3-S6). As determined from the single crystal structure, $B_{12}(OCH_3)_{12}$ crystallizes in a trigonal $R\bar{3}$ space group. Considering that the single crystal measurements were collected at 100 K, we performed additional X-ray diffraction measurements on powder samples at room temperature in order to elucidate structural features under more relevant ambient conditions. An *ab initio* structure solution was obtained via Rietveld refinement of experimental powder data of $B_{12}(OCH_3)_{12}$. Temperature has a significant effect on the unit cell of $B_{12}(OCH_3)_{12}$, as evident by the 0.6% lattice expansion when comparing the structure as determined from powder data (295 K) versus single crystal data (100 K). Despite this, the structure determined via refinement of the powder data shows excellent agreement with the single crystal structure (Figure 3; SI, Figure S30 and Table S1-S8). In the single crystal data, the cluster shows average bond distances of 1.85 Å (B-B), 1.39 Å (B-O), and 1.42 Å (O-C), in line with observed bond distances for other $B_{12}(OR)_{12}$ clusters[96-97, 104] and simulated values[116] for neutral $B_{12}(OCH_3)_{12}$.

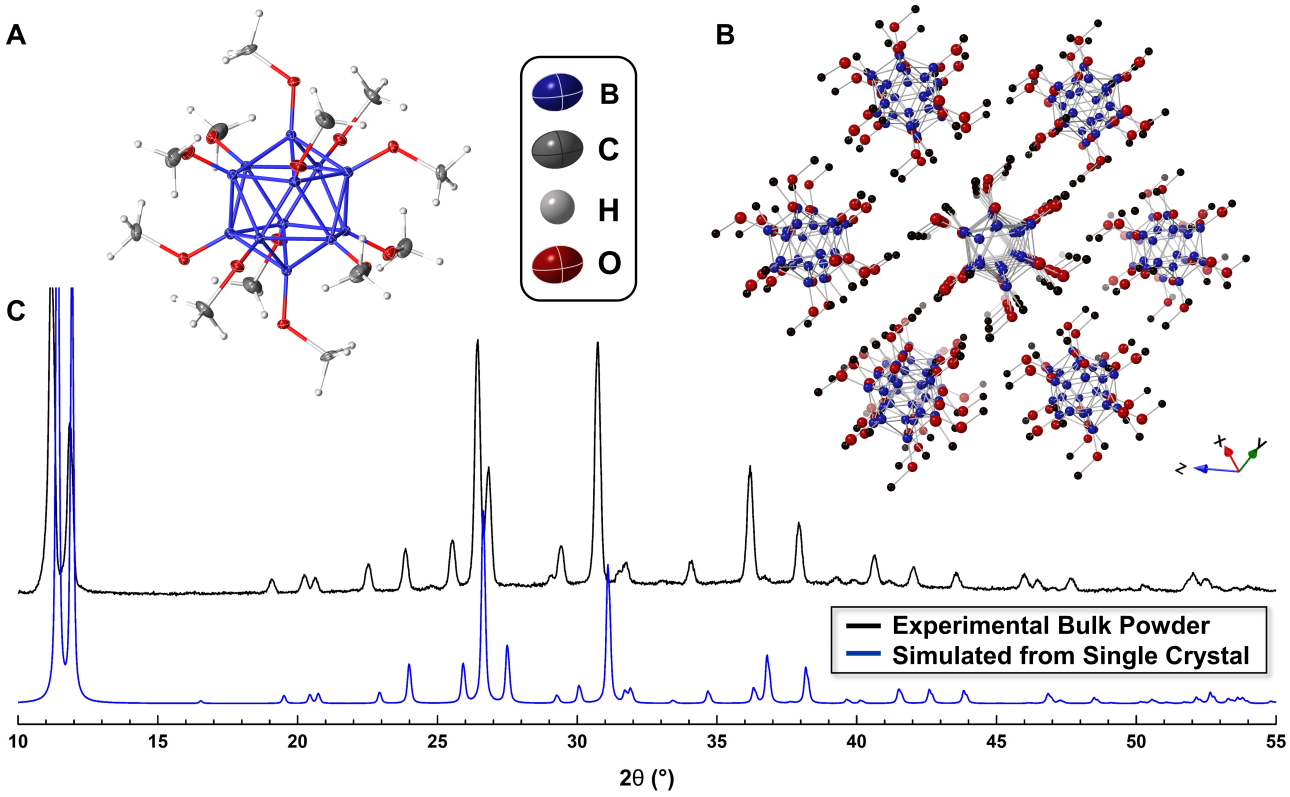

Figure 3. (A) Single crystal structure of $B_{12}(OCH_3)_{12}$ (non-hydrogen atoms depicted as 50% probability ellipsoids; hydrogens depicted as spheres) (B) Extended packing of boron clusters (hydrogens omitted for clarity). (C) Simulated and experimental powder diffraction patterns of $B_{12}(OCH_3)_{12}$.

The packing motif of $B_{12}(OCH_3)_{12}$ as a powder (Figure 3B) shows ample interstitial space (~3 Å cavities between clusters; SI, Figure S32), suggesting the possibility of metal ion insertion. Furthermore, this cluster also shows access to multiple oxidation states in solution (Figure 2C), as well as a radical cationic state, a phenomenon recently observed[102, 107] by our group for many other $B_{12}(OR)_{12}$ clusters. $B_{12}(OCH_3)_{12}$ shows redox activity over a wide voltage window in solution, with half-wave potentials ($E_{1/2}$) spanning a range of more than 1 V, from -0.79 V vs Fc/Fc^+ (2- → 1-) up to +0.89 V (0 → 1+), in good agreement with previous observations of the effect of the R substituent on the redox potentials of $B_{12}(OR)_{12}$ clusters.[96-97, 102, 107] Elucidation of the atomic-level structure

of $B_{12}(OCH_3)_{12}$, in combination with the rich redox behavior in solution, further prompted us to test our original hypothesis and explore whether this material would be a viable candidate for a solid state electrochemical cell.

A model solid state Li-ion cell was constructed with $B_{12}(OCH_3)_{12}$ as the active cathode material (see SI for details), and cyclic voltammetry of the $B_{12}(OCH_3)_{12}$/PEO-SPE/Li cell was performed (Figure 4A). PEO was chosen as the solid electrolyte owing to its high Li-ion conductivity at moderate temperature, flexibility, easy cell fabrication, excellent chemical stability, and high electrochemical stability in the potential window of interest. The cell was first subjected to a cathodic scan starting from its open circuit potential (OCP) of 3.4 V to 1.5 V, followed by an anodic sweep to 4.15 V. The lower and upper voltage limits were chosen to avoid contributions from lithium intercalation into carbon and oxidative decomposition of PEO, respectively. During the cathodic sweep (Figure 4A), significant Faradaic current flow started around 3.40 V to form a broad reduction peak centered around 3.30 V. During the anodic sweep, the corresponding oxidation peak appeared at 3.60 V. Thus, the half wave potential is roughly 3.45 V vs. Li^+/Li, in excellent agreement with the expected value for the $[B_{12}(OCH_3)_{12}]^0/[B_{12}(OCH_3)_{12}]^{1-}$ redox couple, suggesting successful lithiation and delithiation (SI, Figure S27).

The phenomenon suggested by this data is unprecedented for boron clusters in the solid state. Namely, that Li-ions can reversibly intercalate into the cathode during discharge, reducing neutral $B_{12}(OCH_3)_{12}$ clusters to their monoanionic state, followed by a reversal of this process during charging. $E_{1/2}$ remained the same in the subsequent cycles, although a gradual increase of the peak current in the first few cycles was noted. This data suggested a steady increase in the utilization of the active material with cycling due to a gradual wetting of the electrode with the

polymer electrolyte, as observed in PEO-based solid state cells.[117-118] Additionally, the ratio of integrated charge under the reduction and oxidation peaks (i.e., Coulombic efficiency) increased from 78% to 95%. The lower efficiency in the initial cycle can be attributed to the formation of a solid electrolyte interface (SEI) on both the positive and negative electrodes. Once a stable SEI was formed, however, a remarkable Coulombic efficiency of 95% was achieved, signifying highly reversible redox behavior of the boron cluster in the solid state, a crucial prerequisite for use as a battery-active material.

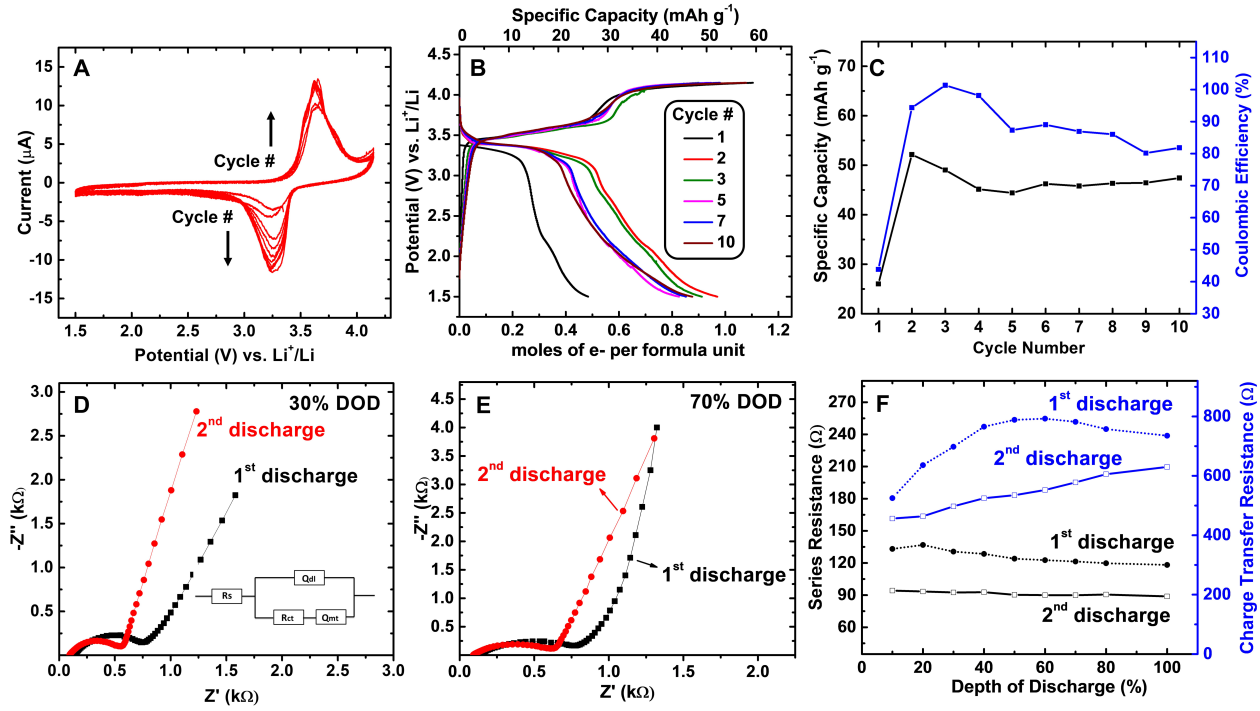

Figure 4. (A) Cyclic voltammetry of a $B_{12}(OCH_3)_{12}$/PEO-SPE/Li cell at 0.1 mV s^{-1}. (B) Galvanostatic cycling at C/20 rate. (C) Variation in specific capacity and Coulombic efficiency with cycle number. (D) Nyquist plots at 30% DOD and (E) 70% DOD. (F) Variation in series and charge transfer resistances with DOD during the first two discharge steps. All measurements were performed at 60°C.

To further demonstrate the utility of this boron cluster for solid state battery applications, galvanostatic cycling was carried out at a C/20 rate (C-rate is based on 1 e^- transfer per formula unit). The specific capacity based on a 1 e- redox process was 53 mAh g^{-1}. Although only 50% of the theoretical capacity was obtained in the first discharge, a theoretical capacity of 95% and a high coulombic efficiency of 96% were observed in the second cycle (Figure 4B and 4C), consistent with the gradual rise of peak current observed during cyclic voltammetry (Figure 4A). The cell also showed high cycling stability, retaining 48 mAh g^{-1} even after ~16 days of cycling (10 cycles at C/20 rate). Measurements were also performed at numerous C-rates and for more cycles (SI, Figure S25 and S26). The charge and discharge curves maintained similar voltage plateaus and sloped regions in all cycles, indicating similar reaction pathways throughout the cycling. Post-mortem XPS of a discharged cell suggests the presence of intact $B_{12}(OCH_3)_{12}$-based clusters in a reduced oxidation state (SI, Figure S24). Unlike traditional all-solid-state cells, which often show significant capacity decay in the first few cycles,[119] the high interfacial stability and intimate contact between the boron cluster electrode and the flexible polymer solid electrolyte is primarily responsible for the remarkable reversibility and capacity retention.

Electrochemical impedance spectroscopy (EIS) was carried out at different depths of discharge (DOD) during the first and second discharge steps to probe the variation in the internal resistance of the cell during cycling. Nyquist plots in the range of 100 kHz to 0.1 Hz show a depressed semicircle at high to medium frequency and an inclined line in the low frequency region (Figure 4D and 4E). The diameter of the semicircle is smaller in the second discharge at both 30% and 70% DOD, indicating a lowered resistance for the charge transfer process at the electrode/electrolyte interface. We also modeled the Nyquist plots using an equivalent circuit, $R_s(Q_{dl}(R_{ct}Q_{mt}))$ where R_s is series resistance, R_{ct} is charge transfer resistance, Q_{dl} and Q_{mt} are the

constant phase elements representing double layer capacitance and mass transfer process, respectively (Figure 4D, inset). The constant phase element (Q) substituted an ideal capacitor (C), in consideration of the distributed capacitive elements of the porous electrode.[120] The series resistance (R_s) included the sum of resistance contributions from the electrolyte, current collectors, and electrodes. R_s = ~120 Ω at all values of DOD in the first discharge and is reduced to ~90 Ω in the second discharge (Figure 4F). This decrease in R_s with cycle number indicates improved interfacial contact and electrode wetting during cycling.[117-118] Similarly, the charge transfer resistance (R_{ct}) at all levels of lithiation in the second cycle is lower than that of the first cycle. For instance, at 50% DOD, R_{ct} = 800 Ω in the first discharge, whereas it is only 550 Ω in the second cycle (Figure 4F). The lower values of both R_s and R_{ct} in the second cycle reduce the overall internal resistance of the cell, leading to better utilization of the electrode and higher capacity.

In order to probe the structure and electrochemistry of the lithiated boron cluster, which was presumably formed during cycling as an electrochemically derived intermediate, we independently synthesized the reduced cluster in the dianionic state with a lithium cation, $Li_2[B_{12}(OCH_3)_{12}]$, and tested it in an identical electrochemical cell (see SI for details). The lithiated cluster was synthesized in good yield through a simple reduction of the neutral cluster in solution with methyl lithium, which proceeded to the fully reduced dianionic cluster. Solution-phase ^{11}B, ^{1}H, and ^{7}Li NMR confirmed the presence of $[B_{12}(OCH_3)_{12}]^{2-}$ with lithium cations (SI, Figure S11-13). Additionally, the reduction of the cluster from 0 to 2- could be observed via X-ray photoelectron spectroscopy (XPS) as a decrease of 1.0 eV in the binding energy of boron 1s electrons (SI, Figure S22), in excellent agreement with our previous observations of an ~0.5 eV shift per each one electron reduction of $B_{12}(OR)_{12}$.[97, 107] Unfortunately, the cell containing $Li_2[B_{12}(OCH_3)_{12}]$ showed inferior electrochemical performance compared to that using neutral

$B_{12}(OCH_3)_{12}$ (Figure S28). Attempts were made to refine the synchrotron data of $Li_2[B_{12}(OCH_3)_{12}]$, but a $LiOH{\cdot}H_2O$ impurity phase was identified which precluded thorough analysis (SI, Figure S31). There are a number of potential reasons for the observed poor solid state cycling behavior and large voltage hysteresis when the chemically lithiated cluster is used as a cathode material. It is anticipated that the presence of the ionically and electronically insulating impurity phase could reduce the overall crystallinity, as well as impede the electron and Li-ion mobility in the lattice, leading to poor electrochemical performance.

CONCLUSION: We have demonstrated the first example of a boron cluster undergoing reversible redox processes in the solid state. Through careful consideration of desirable properties, including low molecular weight, multiple redox events, and sterically accessible ether groups, a methoxy-functionalized boron cluster—$B_{12}(OCH_3)$—was identified as an ideal candidate and synthesized using a microwave reactor. After observing electrochemical behavior in solution, this cluster was then incorporated into an all-solid-state Li-ion cell with a PEO solid electrolyte. The cell could be cycled to utilize 95% of the active material at C/20 rate, with high Coulombic efficiency of 96% and reversibility, retaining 96% of the initial capacity even after 16 days of cycling. Overall, this work represents an important departure from the status quo in cathode material design, opening up a new class of materials for this application. Further improvements for this class of materials can be achieved either by incorporating redox-active cations[121] or reducing the molecular weight of the cluster through the use of smaller polyhedral borane cores.[13, 15, 19, 38] The continued success of this approach will rely on further reducing the molecular weight of the redox-active boron clusters, as well as developing well-defined design rules that govern the interactions between the redox-active anions and cations.

ASSOCIATED CONTENT

Supporting Information

The Supporting Information is available free of charge at https://pubs.acs.org/doi/xxxxx.

General information, synthetic procedures, and characterization data (PDF)

$B_{12}(OCH_3)_{12}$ crystallographic information file (CIF) and checkCIF (PDF)

Crystallographic data are available from the Cambridge Crystallographic Data Centre, under the reference number: CCDC 2239297

AUTHOR INFORMATION

Corresponding Authors

*E-mail: spokoyny@chem.ucla.edu; srnaraya@usc.edu

Author Contributions

The manuscript was written through contributions of all authors. All authors have given approval to the final version of the manuscript.

ACKNOWLEDGMENTS

This work was supported as part of the Center for Synthetic Control Across Length Scales for Advancing Rechargeables (SCALAR), an Energy Frontier Research Center funded by the U.S. Department of Energy, Office of Science, Basic Energy Sciences under Award DE-SC0019381.

The research reported here made use of shared facilities of the UC Santa Barbara Materials Research Science and Engineering Center (MRSEC, NSF DMR 1720256), a member of the Materials Research Facilities Network (http://www.mrfn.org) and the Advanced Photon Source at Argonne National Laboratory, which was supported by the U. S. Department of Energy, Office of Science, Office of Basic Energy Sciences, under Contract No. DE-AC02-06CH11357. A. M.S. thanks NSF Grant CHE-1846849 (NSF CAREER Award) and the Dreyfus Foundation for the Camille Dreyfus Teacher-Scholar Award for additional support. Authors thank Dr. Ignacio Martini for assistance with XPS and Ms. Yessica Nelson for assistance with NMR spectroscopy.

REFERENCES

(1) Gannett, C. N.; Melecio-Zambrano, L.; Theibault, M. J., et al., Organic electrode materials for fast-rate, high-power battery applications. *Materials Reports: Energy,* **2021,** *1* (1), 100008.

(2) Liang, Y.; Tao, Z.; Chen, J., Organic Electrode Materials for Rechargeable Lithium Batteries. *Adv. Energy Mater.,* **2012,** *2* (7), 742-769.

(3) Liang, Y.; Yao, Y., Positioning Organic Electrode Materials in the Battery Landscape. *Joule,* **2018,** *2* (9), 1690-1706.

(4) Lyu, H.; Sun, X.-G.; Dai, S., Organic Cathode Materials for Lithium-Ion Batteries: Past, Present, and Future. *Adv. Energy Sustainability Res.,* **2021,** *2* (1), 2000044.

(5) Muench, S.; Wild, A.; Friebe, C., et al., Polymer-Based Organic Batteries. *Chem. Rev.,* **2016,** *116* (16), 9438-9484.

(6) Schon, T. B.; McAllister, B. T.; Li, P.-F.; Seferos, D. S., The rise of organic electrode materials for energy storage. *Chem. Soc. Rev.,* **2016,** *45* (22), 6345-6404.

(7) Song, Z.; Zhou, H., Towards sustainable and versatile energy storage devices: an overview of organic electrode materials. *Energy & Environmental Science,* **2013,** *6* (8), 2280-2301.

(8) Xie, J.; Zhang, Q., Recent Progress in Multivalent Metal (Mg, Zn, Ca, and Al) and Metal-Ion Rechargeable Batteries with Organic Materials as Promising Electrodes. *Small,* **2019,** *15* (15), 1805061.

(9) Núñez, R.; Tarrés, M.; Ferrer-Ugalde, A., et al., Electrochemistry and Photoluminescence of Icosahedral Carboranes, Boranes, Metallacarboranes, and Their Derivatives. *Chem. Rev.,* **2016,** *116* (23), 14307-14378.

(10) Morris, J. H.; Gysling, H. J.; Reed, D., Electrochemistry of boron compounds. *Chem. Rev.,* **1985,** *85* (1), 51-76.

(11) Grimes, R. N. *Carboranes*. 2 ed.; Academic Press, 2011, pp 985-1019.

(12) Pospíšil, L. r.; King, B. T.; Michl, J., Voltammetry in benzene using lithium dodecamethylcarba-closo-dodecaborate, $LiCB_{11}Me_{12}$, as a supporting electrolyte: reduction of Ag^{+}. *Electrochim. Acta,* **1998,** *44* (1), 103-108.

(13) Axtell, J. C.; Kirlikovali, K. O.; Jung, D., et al., Metal-Free Peralkylation of the closo-Hexaborate Anion. *Organometallics,* **2017,** *36* (6), 1204-1210.

(14) Axtell, J. C.; Saleh, L. M. A.; Qian, E. A., et al., Synthesis and Applications of Perfunctionalized Boron Clusters. *Inorg. Chem.,* **2018,** *57* (5), 2333-2350.

(15) Bykov, A. Y.; Zhdanov, A. P.; Zhizhin, K. Y.; Kuznetsov, N. T., Structure, physicochemical properties, and reactivity of the $[B_9H_9]^{2-}$ anion. *Russ. J. Inorg. Chem.,* **2016,** *61* (13), 1629-1648.

(16) Peymann, T.; Knobler, C. B.; Khan, S. I.; Hawthorne, M. F., Dodecamethyl-closo-dodecaborate(2−). *Inorg. Chem.,* **2001,** *40* (6), 1291-1294.

(17) Preetz, W.; Peters, G., The Hexahydro-closo-hexaborate Dianion $[B_6H_6]^{2-}$ and Its Derivatives. *Eur. J. Inorg. Chem.,* **1999,** *1999* (11), 1831-1846.

(18) Ivanov, S. V.; Miller, S. M.; Anderson, O. P., et al., Synthesis and Stability of Reactive Salts of Dodecafluoro-closo-dodecaborate(2−). *J. Am. Chem. Soc.,* **2003,** *125* (16), 4694-4695.

(19) Li, X.; Yang, T.; Zhou, J., Synergetic ligand and size effects of boron cage based electrolytes in Li-ion batteries. *Phys. Chem. Chem. Phys.,* **2022,** *24* (18), 11345-11352.

(20) Hawthorne, M. F.; Shelly, K.; Li, F., The versatile chemistry of the $[B_{20}H_{18}]^{2-}$ ions: novel reactions and structural motifs. *Chem. Commun.,* **2002,** (6), 547-554.

(21) Wahab, A.; Stepp, B.; Douvris, C., et al., Measured and Calculated Oxidation Potentials of 1-X-12-Y-$CB_{11}Me_{10}^-$ Anions. *Inorg. Chem.,* **2012,** *51* (9), 5128-5137.

(22) Ivanov, S.; Casteel, W.; Pez, G.; Ulman, M. Polyfluorinated boron cluster anions for lithium electrolytes. US 20050064288A1, 2005.

(23) Schlaikjer, C. R. Electrochemical cell with clovoborate salt in electrolyte and method of operation and composition of matter. 4,020,240, 1975.

(24) Wiersema, R. J.; Middaugh, R. L., Electrochemical preparation and halogenation of 1,1'-μ-hydro-bis(undecahydro-closo-dodecaborate)(3-), $B_{24}H_{23}^{3-}$. *Inorg. Chem.,* **1969,** *8* (10), 2074-2079.

(25) Bowden, W., Electrochemical Oxidation of Polyhedral Boron Halide Anions. *J. Electrochem. Soc.,* **1982,** *129* (6), 1249.

(26) Wiersema, R.; Middaugh, R. L., Electrochemical oxidation of $B_{12}H_{12}^{2-}$. *J. Am. Chem. Soc.,* **1967,** *89* (19), 5078-5078.

(27) Middaugh, R.; Farha Jr, F., Kinetics of Electrochemical Oxidative Coupling of Decahydroclovodecaborate (2-) in Acetonitrile. *J. Am. Chem. Soc.,* **1966,** *88* (18), 4147-4149.

(28) Zhang, J.; Fu, X.; Lin, Z.; Xie, Z., Supercarborane Radical Anions with 2n + 3 Electron Counts: A Combined Experimental and Theoretical Study. *Inorg. Chem.,* **2015,** *54* (4), 1965-1973.

(29) Kaczmarczyk, A.; Kolski, G. B.; Townsend, W. P., Oxidative Degradation of Polyhedral Boranes. *J. Am. Chem. Soc.,* **1965,** *87* (6), 1413-1413.

(30) Klanberg, F.; Eaton, D. R.; Guggenberger, L. J.; Muetterties, E. L., Chemistry of boranes. XXVIII. New polyhedral borane anions, $B_8H_8^{2-}$, $B_8H_8^-$, and $B_7H_7^{2-}$. *Inorg. Chem.,* **1967,** *6* (7), 1271-1281.

(31) Boeré, R. T.; Kacprzak, S.; Keßler, M., et al., Oxidation of closo-$[B_{12}Cl_{12}]^{2-}$ to the Radical Anion $[B_{12}Cl_{12}]^-$ and to Neutral $B_{12}Cl_{12}$. *Angew. Chem. Int. Ed.,* **2011,** *50* (2), 549-552.

(32) Lee, T. B.; McKee, M. L., Redox Energetics of Hypercloso Boron Hydrides B_nH_n (n = 6–13) and $B_{12}X_{12}$ (X = F, Cl, OH, and CH_3). *Inorg. Chem.,* **2012,** *51* (7), 4205-4214.

(33) Jelliss, P. A.; Mason, J.; Nazzoli, J. M., et al., Synthesis and Characterization of Ruthenacarborane Complexes Incorporating Chelating N-Donor Ligands: Unexpected Luminescence from the Complex [3-CO-3,3-{κ^2-$Me_2N(CH_2)_2NMe_2$}-closo-3,1,2-$RuC_2B_9H_{11}$]. *Inorg. Chem.,* **2006,** *45* (1), 370-385.

(34) Wiersema, R. J.; Hawthorne, M. F., Electrochemistry and boron-11 nuclear magnetic resonance spectra of monocarbon carboranes. *Inorg. Chem.,* **1973,** *12* (4), 785-788.

(35) Speiser, B.; Tittel, C.; Einholz, W.; Schäfer, R., Redox reactions of the boron subhalide clusters $B_nCl_n^{0/-/2-}$ (n = 8 or 9) investigated by electrochemical and spectroscopic methods. *J. Chem. Soc., Dalton Trans.,* **1999,** (11), 1741-1752.

(36) Speiser, B.; Wizemann, T.; Würde, M., Two-Electron-Transfer Redox Systems, Part 7: Two-Step Electrochemical Oxidation of the Boron Subhalide Cluster Dianions (X = Cl, Br, I). *Inorg. Chem.,* **2003,** *42* (13), 4018-4028.

(37) Einholz, W.; Vaas, K.; Wieloch, C., et al., Chemische und cyclovoltammetrische Untersuchung der Redoxreaktionen der Decahalogendecaborate closo-$[B_{10}X_{10}]^{2-}$ und hypercloso-$[B_{10}X_{10}]^{\cdot -}$ (X=Cl, Br). Kristallstrukturanalyse von $Cs_2[B_{10}Br_{10}]\cdot 2H_2O$. *Zeitschrift für anorganische und allgemeine Chemie,* **2002,** *628* (1), 258-268.

(38) Guschlbauer, J.; Shaughnessy, K. H.; Pietrzak, A., et al., [closo-$B_{10}H_8$-1,10-$(CN)_2]^{2-}$ as a Conduit of Electronic Effects: Comparative Studies of Fe···Fe Communication in [{(η^5-Cp)(dppe)Fe}$_2${μ^2-(NC-X-CN)}]$^{n+}$ (n = 0, 2). *Organometallics,* **2021,** *40* (15), 2504-2515.

(39) Ringstrand, B.; Kaszynski, P.; Young, V. G., Jr.; Janoušek, Z., Anionic Amino Acid [closo-1-CB_9H_8-1-COO-10-$NH_3]^-$ and Dinitrogen Acid [closo-1-CB_9H_8-1-COOH-10-N_2] as Key

Precursors to Advanced Materials: Synthesis and Reactivity. *Inorg. Chem.,* **2010,** *49* (3), 1166-1179.

(40) Wedge, T. J.; Herzog, A.; Huertas, R., et al., Metal−Metal Communication through Carborane Cages Supporting Electroactive [η^5-CpFe(CO)$_2$] Substituents. *Organometallics,* **2004,** *23* (3), 482-489.

(41) Fabre, B.; Clark, J. C.; Vicente, M. G. H., Synthesis and Electrochemistry of Carboranylpyrroles. Toward the Preparation of Electrochemically and Thermally Resistant Conjugated Polymers. *Macromolecules,* **2006,** *39* (1), 112-119.

(42) Mercer, G. D.; Lang, J.; Reed, R.; Scholer, F. R., Electrolytic Reduction of B-Oxy Derivatives of 2,3-Dicarba-closo-undecaborane(11). *Inorg. Chem.,* **1975,** *14* (4), 761-763.

(43) Teixidor, F.; Pedrajas, J.; Vinas, C., Cathodic Cleavage of CS and CP in Carboranyl Derivatives. *Inorg. Chem.,* **1995,** *34*, 1726-1729.

(44) King, B. T.; Körbe, S.; Schreiber, P. J., et al., The Sixteen $CB_{11}H_nMe_{12-n}^-$ Anions with Fivefold Substitution Symmetry: Anodic Oxidation and Electronic Structure. *J. Am. Chem. Soc.,* **2007,** *129* (43), 12960-12980.

(45) Malischewski, M.; Bukovsky, E. V.; Strauss, S. H.; Seppelt, K., Jahn–Teller Effect in the $B_{12}F_{12}$ Radical Anion and Energetic Preference of an Octahedral $B_6(BF_2)_6$ Cluster Structure over an Icosahedral Structure for the Elusive Neutral $B_{12}F_{12}$. *Inorg. Chem.,* **2015,** *54* (23), 11563-11566.

(46) Dey, A. N.; Miller, J., Primary Li / $SOCl_2$ Cells: VII . Effect of and Electrolyte Salts on the Performance. *J. Electrochem. Soc.,* **1979,** *126* (9), 1445.

(47) Johnson, J. W.; Brody, J. F., Lithium Closoborane Electrolytes: III . Preparation and Characterization. *J. Electrochem. Soc.,* **1982,** *129* (10), 2213.

(48) Johnson, J. W.; Whittingham, M. S., Lithium Closoboranes as Electrolytes in Solid Cathode Lithium Cells. *J. Electrochem. Soc.,* **1980,** *127* (7), 1653.

(49) Johnson, J. W.; Thompson, A. H., Lithium Closoboranes II . Stable Nonaqueous Electrolytes for Elevated Temperature Lithium Cells. *J. Electrochem. Soc.,* **1981,** *128* (4), 932.

(50) McArthur, S. G.; Jay, R.; Geng, L., et al., Below the 12-vertex: 10-vertex carborane anions as non-corrosive, halide free, electrolytes for rechargeable Mg batteries. *Chem. Commun.,* **2017,** *53* (32), 4453-4456.

(51) Sadikin, Y.; Brighi, M.; Schouwink, P.; Černý, R., Superionic Conduction of Sodium and Lithium in Anion-Mixed Hydroborates $Na_3BH_4B_{12}H_{12}$ and $(Li_{0.7}Na_{0.3})_3BH_4B_{12}H_{12}$. *Adv. Energy Mater.,* **2015,** *5* (21), 1501016.

(52) Tang, W. S.; Unemoto, A.; Zhou, W., et al., Unparalleled lithium and sodium superionic conduction in solid electrolytes with large monovalent cage-like anions. *Energy & Environmental Science,* **2015,** *8* (12), 3637-3645.

(53) Teprovich, J. A.; Colón-Mercado, H.; Washington Ii, A. L., et al., Bi-functional $Li_2B_{12}H_{12}$ for energy storage and conversion applications: solid-state electrolyte and luminescent down-conversion dye. *J. Mater. Chem. A,* **2015,** *3* (45), 22853-22859.

(54) Tutusaus, O.; Mohtadi, R.; Arthur, T. S., et al., An Efficient Halogen-Free Electrolyte for Use in Rechargeable Magnesium Batteries. *Angew. Chem. Int. Ed.,* **2015,** *54* (27), 7900-7904.

(55) Udovic, T. J.; Matsuo, M.; Tang, W. S., et al., Exceptional Superionic Conductivity in Disordered Sodium Decahydro-closo-decaborate. *Adv. Mater.,* **2014,** *26* (45), 7622-7626.

(56) Udovic, T. J.; Matsuo, M.; Unemoto, A., et al., Sodium superionic conduction in $Na_2B_{12}H_{12}$. *Chem. Commun.,* **2014,** *50* (28), 3750-3752.

(57) He, L.; Li, H.-W.; Nakajima, H., et al., Synthesis of a Bimetallic Dodecaborate $LiNaB_{12}H_{12}$ with Outstanding Superionic Conductivity. *Chem. Mater.,* **2015,** *27* (16), 5483-5486.

(58) Jørgensen, M.; Jensen, S. R. H.; Humphries, T. D., et al., Hydroxylated closo-Dodecaborates $M_2B_{12}(OH)_{12}$ (M = Li, Na, K, and Cs); Structural Analysis, Thermal Properties, and Solid-State Ionic Conductivity. *J. Phys. Chem. C,* **2020,** *124* (21), 11340-11349.

(59) Jung, D.; Muni, M.; Marin, G., et al., Enhancing cycling stability of tungsten oxide supercapacitor electrodes via a boron cluster-based molecular cross-linking approach. *J. Mater. Chem. A,* **2020,** *8* (35), 18015-18023.

(60) Jung, D.; Saleh, L. M. A.; Berkson, Z. J., et al., A molecular cross-linking approach for hybrid metal oxides. *Nat. Mater.,* **2018,** *17* (4), 341-348.

(61) Ready, A. D.; Becwar, S. M.; Jung, D., et al., Synthesis and structural properties of a 2D Zn(II) dodecahydroxy-closo-dodecaborate coordination polymer. *Dalton Trans.,* **2022,** *51* (30), 11547-11557.

(62) Jørgensen, M.; Hansen, B. R. S.; Lee, Y.-S., et al., Crystal Structures and Energy Storage Properties of Ammine Sodium Decahydro-closo-decaboranes ($Na_2B_{10}H_{10}\cdot nNH_3$, n = 1, 2). *J. Phys. Chem. C,* **2019,** *123* (33), 20160-20166.

(63) Paskevicius, M.; Hansen, B. R. S.; Jørgensen, M., et al., Multifunctionality of silver closo-boranes. *Nat. Commun.,* **2017,** *8* (1), 15136.
(64) Tang, W. S.; Matsuo, M.; Wu, H., et al., Stabilizing lithium and sodium fast-ion conduction in solid polyhedral-borate salts at device-relevant temperatures. *Energy Storage Mater.,* **2016,** *4*, 79-83.
(65) Yoshida, K.; Sato, T.; Unemoto, A., et al., Fast sodium ionic conduction in $Na_2B_{10}H_{10}$-$Na_2B_{12}H_{12}$ pseudo-binary complex hydride and application to a bulk-type all-solid-state battery. *Appl. Phys. Lett.,* **2017,** *110* (10), 103901.
(66) Toyama, N.; Kim, S.; Oguchi, H., et al., Lithium ion conductivity of complex hydrides incorporating multiple closo-type complex anions. *J. Energy Chem.,* **2019,** *38*, 84-87.
(67) Kim, S.; Kisu, K.; Takagi, S., et al., Complex Hydride Solid Electrolytes of the $Li(CB_9H_{10})$–$Li(CB_{11}H_{12})$ Quasi-Binary System: Relationship between the Solid Solution and Phase Transition, and the Electrochemical Properties. *ACS Appl. Energy Mater.,* **2020,** *3* (5), 4831-4839.
(68) Hansen, B. R. S.; Paskevicius, M.; Jørgensen, M.; Jensen, T. R., Halogenated Sodium-closo-Dodecaboranes as Solid-State Ion Conductors. *Chem. Mater.,* **2017,** *29* (8), 3423-3430.
(69) Sadikin, Y.; Schouwink, P.; Brighi, M., et al., Modified Anion Packing of $Na_2B_{12}H_{12}$ in Close to Room Temperature Superionic Conductors. *Inorg. Chem.,* **2017,** *56* (9), 5006-5016.
(70) Duchêne, L.; Kühnel, R. S.; Rentsch, D., et al., A highly stable sodium solid-state electrolyte based on a dodeca/deca-borate equimolar mixture. *Chem. Commun.,* **2017,** *53* (30), 4195-4198.
(71) Tang, W. S.; Yoshida, K.; Soloninin, A. V., et al., Stabilizing Superionic-Conducting Structures via Mixed-Anion Solid Solutions of Monocarba-closo-borate Salts. *ACS Energy Lett.,* **2016,** *1* (4), 659-664.
(72) Payandeh, S.; Asakura, R.; Avramidou, P., et al., Nido-Borate/Closo-Borate Mixed-Anion Electrolytes for All-Solid-State Batteries. *Chem. Mater.,* **2020,** *32* (3), 1101-1110.
(73) Kim, S.; Oguchi, H.; Toyama, N., et al., A complex hydride lithium superionic conductor for high-energy-density all-solid-state lithium metal batteries. *Nat. Commun.,* **2019,** *10* (1), 1081.
(74) Brighi, M.; Murgia, F.; Łodziana, Z., et al., A mixed anion hydroborate/carba-hydroborate as a room temperature Na-ion solid electrolyte. *J. Power Sources,* **2018,** *404*, 7-12.

(75) Asakura, R.; Duchêne, L.; Kühnel, R.-S., et al., Electrochemical Oxidative Stability of Hydroborate-Based Solid-State Electrolytes. *ACS Appl. Energy Mater.,* **2019,** *2* (9), 6924-6930.
(76) Duchêne, L.; Kühnel, R. S.; Stilp, E., et al., A stable 3 V all-solid-state sodium–ion battery based on a closo-borate electrolyte. *Energy & Environmental Science,* **2017,** *10* (12), 2609-2615.
(77) Duchêne, L.; Remhof, A.; Hagemann, H.; Battaglia, C., Status and prospects of hydroborate electrolytes for all-solid-state batteries. *Energy Storage Mater.,* **2020,** *25*, 782-794.
(78) Unemoto, A.; Ikeshoji, T.; Yasaku, S., et al., Stable Interface Formation between TiS_2 and $LiBH_4$ in Bulk-Type All-Solid-State Lithium Batteries. *Chem. Mater.,* **2015,** *27* (15), 5407-5416.
(79) Li, S.; Qiu, P.; Kang, J., et al., Iodine-Substituted Lithium/Sodium closo-Decaborates: Syntheses, Characterization, and Solid-State Ionic Conductivity. *ACS Appl. Mater. Interfaces,* **2021,** *13* (15), 17554-17564.
(80) Černý, R.; Murgia, F.; Brighi, M., Metal hydroborates: From hydrogen stores to solid electrolytes. *J. Alloys Compd.,* **2022,** *895*, 162659.
(81) Tang, W. S.; Matsuo, M.; Wu, H., et al., Liquid-Like Ionic Conduction in Solid Lithium and Sodium Monocarba-closo-Decaborates Near or at Room Temperature. *Adv. Energy Mater.,* **2016,** *6* (8), 1502237.
(82) Cuan, J.; Zhou, Y.; Zhou, T., et al., Borohydride-Scaffolded Li/Na/Mg Fast Ionic Conductors for Promising Solid-State Electrolytes. *Adv. Mater.,* **2019,** *31* (1), 1803533.
(83) H. P. Souza, D.; Møller, K. T.; Moggach, S. A., et al., Hydrated alkali-$B_{11}H_{14}$ salts as potential solid-state electrolytes. *J. Mater. Chem. A,* **2021,** *9* (26), 15027-15037.
(84) Lu, Z.; Ciucci, F., Metal Borohydrides as Electrolytes for Solid-State Li, Na, Mg, and Ca Batteries: A First-Principles Study. *Chem. Mater.,* **2017,** *29* (21), 9308-9319.
(85) Dimitrievska, M.; Wu, H.; Stavila, V., et al., Structural and Dynamical Properties of Potassium Dodecahydro-monocarba-closo-dodecaborate: $KCB_{11}H_{12}$. *J. Phys. Chem. C,* **2020,** *124* (33), 17992-18002.
(86) Sadikin, Y.; Skoryunov, R. V.; Babanova, O. A., et al., Anion Disorder in $K_3BH_4B_{12}H_{12}$ and Its Effect on Cation Mobility. *J. Phys. Chem. C,* **2017,** *121* (10), 5503-5514.
(87) Niitani, K.; Ushiroda, S.; Kuwata, H., et al., Hard Carbon Anode with a Sodium Carborane Electrolyte for Fast-Charging All-Solid-State Sodium-Ion Batteries. *ACS Energy Lett.,* **2022,** *7* (1), 145-149.

(88) Keener, M.; Mattejat, M.; Zheng, S.-L., et al., Selective electrochemical capture and release of uranyl from aqueous alkali, lanthanide, and actinide mixtures using redox-switchable carboranes. *Chem. Sci.,* **2022,** *13* (12), 3369-3374.

(89) Keener, M.; Hunt, C.; Carroll, T. G., et al., Redox-switchable carboranes for uranium capture and release. *Nature,* **2020,** *577* (7792), 652-655.

(90) Michl, J., Chemistry of the three-dimensionally aromatic CB_{11} cage. *Pure Appl. Chem.,* **2008,** *80* (3), 429-446.

(91) Fete, M. G.; Havlas, Z.; Michl, J., $HCB_{11}(CF_3)_nF_{11-n}^-$: Inert Anions with High Anodic Oxidation Potentials. *J. Am. Chem. Soc.,* **2011,** *133* (11), 4123-4131.

(92) Boeré, R. T.; Derendorf, J.; Jenne, C., et al., On the Oxidation of the Three-Dimensional Aromatics $[B_{12}X_{12}]^{2-}$ (X=F, Cl, Br, I). *Chem. Eur. J.,* **2014,** *20* (15), 4447-4459.

(93) Bukovsky, E. V.; Peryshkov, D. V.; Wu, H., et al., Comparison of the Coordination of $B_{12}F_{12}^{2-}$, $B_{12}Cl_{12}^{2-}$, and $B_{12}H_{12}^{2-}$ to Na^+ in the Solid State: Crystal Structures and Thermal Behavior of $Na_2(B_{12}F_{12})$, $Na_2(H_2O)_4(B_{12}F_{12})$, $Na_2(B_{12}Cl_{12})$, and $Na_2(H_2O)_6(B_{12}Cl_{12})$. *Inorg. Chem.,* **2017,** *56* (8), 4369-4379.

(94) Lacroix, M. R.; Bukovsky, E. V.; Lozinšek, M., et al., Manifestations of Weak O–H···F Hydrogen Bonding in $M(H_2O)_n(B_{12}F_{12})$ Salt Hydrates: Unusually Sharp Fourier Transform Infrared ν(OH) Bands and Latent Porosity (M = Mg–Ba, Co, Ni, Zn). *Inorg. Chem.,* **2018,** *57* (23), 14983-15000.

(95) Qian, E. A.; Wixtrom, A. I.; Axtell, J. C., et al., Atomically precise organomimetic cluster nanomolecules assembled via perfluoroaryl-thiol SNAr chemistry. *Nat. Chem.,* **2017,** *9* (4), 333-340.

(96) Wixtrom, A. I.; Shao, Y.; Jung, D., et al., Rapid synthesis of redox-active dodecaborane $B_{12}(OR)_{12}$ clusters under ambient conditions. *Inorg. Chem. Front.,* **2016,** *3* (5), 711-717.

(97) Wixtrom, A. I.; Parvez, Z. A.; Savage, M. D., et al., Tuning the electrochemical potential of perfunctionalized dodecaborate clusters through vertex differentiation. *Chem. Commun.,* **2018,** *54* (46), 5867-5870.

(98) Shida, N.; Owaki, S.; Eguchi, H., et al., Bis(pentafluorophenyl)-o-carborane and its arylthio derivatives: synthesis, electrochemistry and optical properties. *Dalton Trans.,* **2020,** *49* (37), 12985-12989.

(99) Farha, O. K.; Julius, R. L.; Lee, M. W., et al., Synthesis of Stable Dodecaalkoxy Derivatives of hypercloso-$B_{12}H_{12}$. *J. Am. Chem. Soc.,* **2005,** *127* (51), 18243-18251.
(100) Hawthorne, M. F.; Pushechnikov, A., Polyhedral borane derivatives: Unique and versatile structural motifs. *Pure Appl. Chem.,* **2012,** *84* (11), 2279-2288.
(101) Lee, M. W.; Farha, O. K.; Hawthorne, M. F.; Hansch, C. H., Alkoxy Derivatives of Dodecaborate: Discrete Nanomolecular Ions with Tunable Pseudometallic Properties. *Angew. Chem. Int. Ed.,* **2007,** *46* (17), 3018-3022.
(102) Li, B.; Zhang, X.; Stauber, J. M., et al., Electronic Structure of Superoxidized Radical Cationic Dodecaborate-Based Clusters. *J. Phys. Chem. A,* **2021,** *125* (28), 6141-6150.
(103) Messina, M. S.; Axtell, J. C.; Wang, Y., et al., Visible-Light-Induced Olefin Activation Using 3D Aromatic Boron-Rich Cluster Photooxidants. *J. Am. Chem. Soc.,* **2016,** *138* (22), 6952-6955.
(104) Peymann, T.; Knobler, C. B.; Khan, S. I.; Hawthorne, M. F., Dodeca(benzyloxy)dodecaborane, $B_{12}(OCH_2Ph)_{12}$: A Stable Derivative of hypercloso-$B_{12}H_{12}$. *Angew. Chem. Int. Ed.,* **2001,** *40* (9), 1664-1667.
(105) Spokoyny, A. M., New ligand platforms featuring boron-rich clusters as organomimetic substituents. *Pure Appl. Chem.,* **2013,** *85* (5), 903.
(106) Stauber, J. M.; Qian, E. A.; Han, Y., et al., An Organometallic Strategy for Assembling Atomically Precise Hybrid Nanomaterials. *J. Am. Chem. Soc.,* **2020,** *142* (1), 327-334.
(107) Stauber, J. M.; Schwan, J.; Zhang, X., et al., A Super-Oxidized Radical Cationic Icosahedral Boron Cluster. *J. Am. Chem. Soc.,* **2020,** *142* (30), 12948-12953.
(108) Barton, J. L.; Wixtrom, A. I.; Kowalski, J. A., et al., Perfunctionalized Dodecaborate Clusters as Stable Metal-Free Active Materials for Charge Storage. *ACS Appl. Energy Mater.,* **2019,** *2* (7), 4907-4913.
(109) Kim, Y.; Kubena, R.; Axtell, J., et al., Dynamic Nuclear Polarization Using 3D Aromatic Boron Cluster Radicals. *J. Phys. Chem. Lett.,* **2021,** *12* (1), 13-18.
(110) Qian, E. A.; Han, Y.; Messina, M. S., et al., Multivalent Cluster Nanomolecules for Inhibiting Protein–Protein Interactions. *Bioconjugate Chem.,* **2019,** *30* (10), 2594-2603.
(111) Axtell, J. C.; Messina, M. S.; Liu, J.-Y., et al., Photooxidative Generation of Dodecaborate-Based Weakly Coordinating Anions. *Inorg. Chem.,* **2019,** *58* (16), 10516-10526.

(112) Goswami, L. N.; Everett, T. A.; Khan, A. A.; Hawthorne, M. F., Rational Design of a Stable Two One-Electron Redox-Active closo-Dodecaalkoxyborane Ion as Biothiol Sensor. *Eur. J. Inorg. Chem.,* **2020,** *2020* (4), 377-381.

(113) Aubry, T. J.; Axtell, J. C.; Basile, V. M., et al., Dodecaborane-Based Dopants Designed to Shield Anion Electrostatics Lead to Increased Carrier Mobility in a Doped Conjugated Polymer. *Adv. Mater.,* **2019,** *31* (11), 1805647.

(114) Aubry, T. J.; Winchell, K. J.; Salamat, C. Z., et al., Tunable Dopants with Intrinsic Counterion Separation Reveal the Effects of Electron Affinity on Dopant Intercalation and Free Carrier Production in Sequentially Doped Conjugated Polymer Films. *Adv. Funct. Mater.,* **2020,** *30* (28), 2001800.

(115) Muetterties, E. L.; Balthis, J. H.; Chia, Y. T., et al., Chemistry of Boranes. VIII. Salts and Acids of $B_{10}H_{10}^{2-}$ and $B_{12}H_{12}^{2-}$. *Inorg. Chem.,* **1964,** *3* (3), 444-451.

(116) McKee, M. L., Density Functional Theory Study of Anionic and Neutral Per-Substituted 12-Vertex Boron Cage Systems, $B_{12}X_{12}^{n-}$ (n = 2, 1, 0). *Inorg. Chem.,* **2002,** *41* (5), 1299-1305.

(117) Tan, J.; Ao, X.; Dai, A., et al., Polycation ionic liquid tailored PEO-based solid polymer electrolytes for high temperature lithium metal batteries. *Energy Storage Mater.,* **2020,** *33*, 173-180.

(118) Zhou, W.; Wang, Z.; Pu, Y., et al., Double-Layer Polymer Electrolyte for High-Voltage All-Solid-State Rechargeable Batteries. *Adv. Mater.,* **2019,** *31* (4), 1805574.

(119) Elizalde-Segovia, R.; Irshad, A.; Zayat, B.; Narayanan, S. R., Solid-State Lithium-Sulfur Battery Based on Composite Electrode and Bi-layer Solid Electrolyte Operable at Room Temperature. *J. Electrochem. Soc.,* **2020,** *167* (14), 140529.

(120) Irshad, A.; Elizalde-Segovia, R.; Jayathilake, B. S., et al., Understanding the Role of Carbon Mixtures on the Polarization of Sulfur Electrodes in Lithium-Sulfur Batteries. *J. Electrochem. Soc.,* **2022,** *169* (11), 110528.

(121) Hansen, C. J.; Zak, J. J.; Martinolich, A. J., et al., Multielectron, Cation and Anion Redox in Lithium-Rich Iron Sulfide Cathodes. *J. Am. Chem. Soc.,* **2020,** *142* (14), 6737-6749.

Table of Contents Figure (TOC):

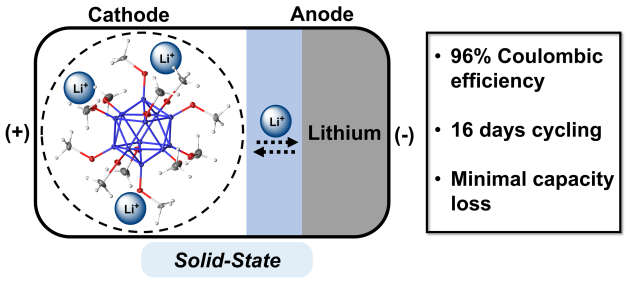

- 96% Coulombic efficiency
- 16 days cycling
- Minimal capacity loss